Journal of Microscopy | RMS

ORIGINAL ARTICLE

Comparison of the effects of AgNPs on the morphological and mechanical characteristics of cancerous cells

Jiajing Zhu[1,2] | **Yanling Tian**[1] | **Liang Cao**[3,4] | **Jing Hu**[3,4] | **Jin Yan**[3,4] | **Zuobin Wang**[3,4] | **Xianping Liu**[1]

[1]School of Engineering, University of Warwick, Coventry, UK

[2]Wheeled System Technology Department, China North Vehicle Research Institute, Beijing, China

[3]International Research Centre for Nano Handling and Manufacturing of China, Changchun University of Science and Technology, Changchun, China

[4]Ministry of Education Key Laboratory for Cross-Scale Micro and Nano Manufacturing, Changchun University of Science and Technology, Changchun, China

Correspondence
Yanling Tian, School of Engineering, University of Warwick, Coventry CV4 7AL, UK.
Email: y.tian.1@warwick.ac.uk

Abstract

Currently, silver nanoparticles (AgNPs) are the most produced nanoparticles in global market and have been widely utilized in the biomedical field. Here, we investigated the morphological and mechanical effects of AgNPs on cancerous cells of A549 cells and SMMC-7721 cells with atomic force microscope (AFM). The influence of AgNPs on the morphological properties and mechanical properties of cancerous cells were characterized utilizing the force–volume (FV) mode and force spectroscopy (FS) mode of AFM measurement. We mainly focus on the comparison of the effects of AgNPs on the two types of cancerous cells based on the fitting results of calculating the Young's moduli utilizing the Sneddon model. The results showed that the morphology changed little, but the mechanical properties of height, roughness, adhesion force and Young's moduli of two cancerous cells varied significantly with the stimulation of different concentrations of AgNPs. This research has provided insights into the classification and characterization of the effects of the various concentrations of AgNPs on the cancerous cells in vitro by utilizing AFM methodologies for disease therapy.

KEYWORDS
AgNPs, atomic force microscope, cancer cells, mechanical properties, morphology

1 | INTRODUCTION

Currently, nanoparticles (NPs) have been a popular nanoscience and nanotechnology with a diameter between 1 and 100 nm by the aggregation of atomics at the nanoscale. The advantages of characteristics of nanoparticles are high reactivity, better stability, updated biological properties, antimicrobial effect with greater therapeutic efficacy and less side effects.[1–3] Nanoparticles have been widely applied in a variety of fields, especially for

biomedical area such as the oncology, bioimaging,[4,5] medication administration systems[6–9] and pharmaceutical industry.[10,11]

Nanoparticles can be classified by various characteristics, including morphological shapes, sizes, materials, chemical composition etc. The morphologies of nanoparticles include cylindrical, spherical, tubular, spiral shape, and irregular shape with the size range from 1 to 100 nm. In terms of materials, the nanoparticles can be divided into metallic NPs and biocomponental NPs. Metallic NPs mainly include the materials of metals and metal oxides, which are most commonly used gold (Au), silver (Ag), copper (Cu), zinc (Zn), aluminium oxide (Al_2O_3), iron oxide (Fe_2O_3), titanium oxide (TiO_2), zinc oxide (ZnO) etc.[12,13] Biocomponental NPs are composed of biocomponents, such as liposomes, lignin, biopolymers, chitosan, micelles.[13,14] Metallic NPs have multiple properties with various size and shapes and metal oxide NPs have better efficiency and reactivity. Biocomponental NPs are widely regarded as biodegradable and non-toxic.

AgNPs are the most produced nanoparticles in global market and have been widely utilized in the biomedical field. Nanoparticles are able to penetrate the cell membranes and interact with cells' internal components.[15] The mechanism of action of AgNPs is the induction of apoptosis and death of cells with high penetrating power by damaging mitochondrial functions and causing gene expression disorders through the scavenger receptor mediated phagocytosis.[16] However, inhibition failure of AgNPs is possibly due to the resistance of cellular structures, such as genetic elements and membrane proteins.[14,17–20] Moreover, AgNPs have been discovered to exhibit good antimicrobial activity against *Mycobacterium tuberculosis*,[21–23] *Pseudomonas aeruginosa* and *Staphylococcus aureus*.[24] The inhibition effects of AgNPs are over 95% for *Pseudomonas aeruginosa* and *Staphylococcus aureus* with biofilms.[25]

In the field of measurement methods, cell morphology and cell mechanics are measured using different methods to characterize the corresponding morphological and mechanical properties. On the one hand, the morphology of cells are generally characterized by optical microscope, scanning electron microscope (SEM)/Focused ion beam (FIB), transmission electron microscope (TEM), atomic force microscope (AFM) etc. In terms of materials, AFM and optical microscope have the ability to measure almost all kinds of multiple materials (especially for living cells) without extra conductive films and long preparation time by comparing to the SEM/FIB and TEM, which may cause less damage to cells and reduce cost.[26,27] In the aspect of imaging resolution, the imaging resolution of AFM (0.1 nm) is similar to that of TEM (0.1–0.5 nm), which are both higher than that of SEM (3–6 nm) and ordinary optical microscope (1 mm).[28,29] With regard to ambient environment requirement, AFM and optical microscope can be carried out in a variety of ambient environments (vacuum, air, liquid) while SEM/TEM measurement can only be utilised in high vacuum environment.[30,31] Therefore, AFM has greater flexible advantages in three-dimensional (3D) topography of living cells with higher resolution because it can operate in physiological environment and maintain the viability of living biological systems, especially for a single cell[32,33] and single molecule.[34–36] On the other hand, the developed methods of cell mechanics mainly comprise the PLR, MTC, CMR, PTM, OS, AFM etc.[36] Among these methods, AFM provides a direct measurement approach of living cells in physiological environment almost non-destructively with higher force sensitivity and resolution accuracy at the atomic level.[37,38]

Here, we investigated the mechanical effects of AgNPs on cancerous cells of A549 cells and SMMC-7721 cells using atomic force microscopy. The effects of AgNPs on the morphological properties of cancerous cells were characterized by using of the force–volume (FV) mode. In addition, the effects of AgNPs on the mechanical properties of cancerous cells were analyzed by force spectroscopy mode. We mainly focus on the comparison of the effects of AgNPs on the two types of cancerous cells with emphasis on the fitting results of calculating the Young's moduli by Sneddon model.

2 | EXPERIMENTAL DETAILS

2.1 | Chemicals

RPMI1640 medium and fetal bovine serum (FBS) were supplied by Hyclone Laboratories Inc. (Canada). Dulbecco's Modified Eagle medium (DMEM), trypsin and phosphate buffer saline (PBS) were produced from Gibco (USA). Amino functionalised silver nanoparticles (AgNPs) with 10–100 nm diameter in citrate buffer were obtained from Aladdin (China).

2.2 | Cell culture

The hepatoma carcinoma cells (SMMC-7721 cells) and lung cancerous cells (A549 cells) were obtained from The Cell Bank of Type Culture Collection of Chinese Academy of Sciences (Shanghai, China). SMMC-7721 cells were cultured in RPMI 1640 medium supplemented with 10% FBS while A549 cells were cultivated in DMEM medium with 10% FBS. Prepared cells were grown in the incubator (IP610, Yamato, Japan) at 37°C with 5% CO_2. Before the experiment, diluted live cells were dispersed on thin sheet glasses in culture dishes with cell densities of 1.0×10^4 cells

for another 24 h cultivation after centrifuging. In order to eliminate impurities and dead cells, PBS was required to wash the experimental samples for triple times and then affiliate the fresh medium solutions.

2.3 | Cell viability assay

The viability rates of A549 cells and SMMC-7721 cells with various concentrations of AgNPs were measured by MTT assay. Microplate spectrophotometer (Epoch 2, BioTek, USA) was used to detect the effects of AgNPs treated SMMC-7721 cells and A549 cells under the OD value of 492 nm. The cells in the logarithmic growth phase were seeded into 96-well plates (Kangning Co., USA) with a density of 1.0×10^4 cells with 100 μl per well and put in an incubator for 24 h at 37°C with 5% CO_2.

The 0.22-μm syringe filter is applied for the AgNPs solutions in order to eliminate the bacteria and impurities. After the ultrasonic concussion for 3 min, AgNPs with an increased concentration were added to the each well with 100 μl for another 24 h cultivation in an incubator. Therefore, the cell culture medium containing AgNPs (0, 0.059, 0.117, 0.234, 0.469, 0.938, 1.875, 3.75, 7.50, 15 μg/ml) was 200 μl in each well. After the stimulation of AgNPs for 24 h, 20 μl of MTT (Sigma-Aldrich, America) was added to each cell well for another 4 h incubation. Following the removing of the supernatant liquid, dimethylsulphoxide (DMSO) was added to each well with 150 μl, the inhibition rates of cell proliferation were examined by MTT assay.

2.4 | Inverted optical microscopy analysis

Inverted optical microscopy (NIKON, Japan) with 10× or 20× optical lens is used for the morphological characterization to provide the real-time dynamic imaging of various live cancerous cells of A549 cells and SMMC-7721 cells. The cells in the logarithmic growth phase were seeded into 96-well plates (Kangning Co., USA) with a density of 1.0×10^4 cells with 100 μl per well and put in an incubator for 24 h at 37°C with 5% CO_2. AgNPs with an increased concentration of 0, 3.25, 7.50 and 15 μg/ml were added to the each well with 100 μl for another 24 h cultivation in the incubator. Therefore, the optical morphological properties of A549 cells and SMMC-7721 cells were observed with the stimulation of AgNPs concentrations of 0 μg/ml, 1.875 μg/ml, 3.75 μg/ml and 7.50 μg/ml.

2.5 | Focused ion beam analysis

A dual focused ion beam/scanning electron microscope, commonly terms as FIB/SEM system (FEI Helios G4 PFIB,

ThermoFisher Scientific, USA), is used to characterize the morphological properties in nano-micro-scale for AgNPs. FIB analysis is implemented in high vacuum (HV) mode of 15 kV with 1.6×10^4 to 1.2×10^5 magnification. AgNPs solution is filtered by 0.22 μm syringe filter and vibrated by the ultrasonic for 3 min in order to eliminate the bacteria and impurities as well as maintain the well-proportioned to avoid the aggregation phenomenon. Then the AgNPs solution of 50 μl is dropped on a clean silicon substrate of 1 cm × 1 cm. Before FIB imaging, the substrate is placed into the ultra-clean workbench platform and waited for the substrate to dry completely.

2.6 | Atomic force microscope analysis

The JPK AFM system (NanoWizard®3, Germany) was employed to record the morphological and mechanical properties of live cells. Force–volume (FV) mode, also described with quantitative imaging (QI) mode, was used to measure the morphology of cells with 256 × 256 pixels. Force spectroscopy (FS) mode was applied to obtain the force–distance curves in nano-indentation experiments. The Young's moduli were calculated from the force–distance curves with Sneddon model. In order to remove the influence of different culture mediums and serum concentrations, PBS was applied to the unified medium solutions during the measurement using JPK system. Before measurement, samples were washed with PBS three times in order to eliminate the dead cells and floating impurities and then added the new PBS solutions for the following measurement. It is also essential to ensure the accuracy of the experimental results by avoiding the rupture or contamination of the probe. All experiments were carried out at the room temperature in a super-clean workbench platform.

The Bruker MLCT A probe with a triangular silicon nitride tip (Bruker Corporation, Santa Barbara, CA) was used for the AFM nano-indentation experiments. The Bruker MLCT A probe has a nominal spring constant of 0.07 N/m and the nominal radius 20 nm. The deflection sensitivity and spring constant were optimized by pushing on the same glass base in liquid without cells for calibration of the probe using thermal tuning. The deflection sensitivity and spring constant for MLCT A probe was calculated to be 17.82 nm/V and 0.072 N/m, respectively.

Based on the JPK force spectroscopy mode, the force–distance curves were obtained by applying the stable force on the central area of cells in order to speculate the internal microstructure changes of cells. The force–distance curves were measured with concentrations of AgNPs of 0 μg/ml, 1.875 μg/ml, 3.75 μg/ml and 7.50 μg/ml, respectively. According to the above AFM morphology results,
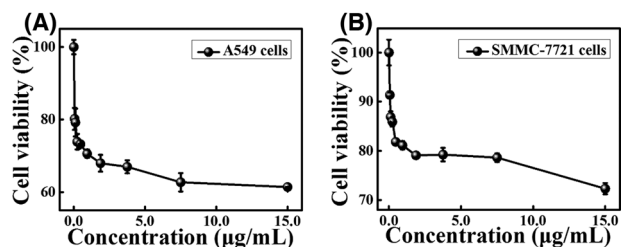
FIGURE 1 Evaluation of cell apoptosis with various concentrations of AgNPs by using the MTT assay. (A) Cell viability of A549 cells after the stimulation of AgNPs for 24 h. (B) Cell viability of SMMC-7721 cells after the stimulation of AgNPs for 24 h.

the stimulation time of AgNPs was finally set to 24 h for nano-indentation test. Moreover, in order to exclude the influence of other measurement parameters, the measurement parameters of indentation force, indentation speed, dwelling time, retraction time and Z length were set to 1.0 nN, 2.0 μm/s, 0.0 s, 0.0 s and 5.0 μm, respectively. Afterwards, the measurement was performed automatically with set value for the manually selected central area of cells. The samples were cleaned with fresh PBS for three times and finally added fresh AgNPs solutions at room temperature for nano-indentation test.

During the measurement process, the cells were chosen by visual observation and basic experience. As investigated in previous research, the general dimension ranges of A549 cells and SMMC-7721 cells are 50–90 μm and 35–55 μm in length, 25–40 μm in width. In order to ensure the validity and consistency of the experimental results, at least 5 force–depth curves were obtained for each cell and at least 10 cells were detected for each sample. Each force–distance curve is carried out in several seconds (1–15 s when the indentation speed is 0.5–5 μm/s), thus the over 50 curves for each sample is usually completed in 10 min.

3 | RESULTS AND DISCUSSION

3.1 | Cell viability

The effects of AgNPs solutions on cell proliferation or apoptosis were measured by MTT assay. After the cell cultivation with a density of 1.0×10^4 cells with 100 μl per well in 96 well plates for 24 h, AgNPs solutions with an increased concentration of 0–30 μg/ml were added to the each well with 100 μl for another 24 h cultivation in an incubator. Finally, the survival rates of cell growth with increasing concentration of 0–15 μg/ml AgNPs solutions were carried out by Microplate Spectrophotometer with the OD value of 492 nm.

As can be seen from Figure 1, the MTT experimental result revealed the effects of various concentrations of

AgNPs on the SMMC-7721 cells and A549 cells after the stimulation with 24 h. It can be observed that the survival rate of SMMC-7721 cells and A549 cells both decreased with the increase of concentrations of AgNPs solutions with filtration. Additionally, the lowest survival rates of A549 cells and SMMC-7721 cells are 61.399% and 72.304% with the concentration of AgNPs at 15 μg/ml. By comparing the effects of the concentrations of AgNPs on the different cancerous cells, the survival rates of A549 cells are slightly lower than that of SMMC-7721 cells. Thus, the inhibitory effects of AgNPs on the SMMC-7721 cells and A549 cells are demonstrated changeable with the different concentrations from the MTT assay result.

The reason for this phenomenon possibly due to the various cancerous cells with complicated intracellular structures may react changeable with the different concentrations of AgNPs. Cell membranes have the ability to penetrate nanoparticles and cell internal components may interact with nanoparticles, which may appeared the possibility to induce destruction of the cell membrane, extract phospholipid molecules from membrane and the apoptosis of cells. Therefore, the A549 cells and SMMC-7721 cells show the decreased viability with the increased concentrations of AgNPs from the MTT assay result.

3.2 | Morphological properties of AgNPs

AgNPs are measured by the HV mode of FIB and FV mode of AFM to investigate the morphological properties, as displayed in Figure 2. Typical FIB images of AgNPs distributions at scale bar of 500 nm with 1.6×10^4 magnification and at scale bar of 200 nm with 1.2×10^5 magnification are shown in Figure 2A and B. The AFM images AgNPs with white scale bar of 1 μm is listed as the Figure 2C, and the yellow square is 300 nm × 300 nm. The statistical distribution of AgNPs corresponding to the whole AFM height map's image and selected statistical section of the yellow square of 300 nm × 300 nm with Gaussian distribution fitting are demonstrated in Figure 2D and E.

As shown in Figure 2A–C, FIB and AFM images reveals the two dimensional topography images and 3D images of smooth spherical AgNPs within the range of 50–100 nm in diameter, displaying uniform in shape and size. It can be observed that the majority height values of AgNPs are 26.24 ± 0.16 nm for the whole image of height map and 18.10 ± 0.62 nm corresponding to the selected statistical section of the yellow square of 300 nm × 300 nm in height map's image, as presented in Figure 2D and E. It is evident that AgNPs without functionalisation will display a common slightly aggregation phenomenon from Figure 2A–C. In the following measurement, various concentrations of AgNPs will be utilized in the two types of cancerous cells
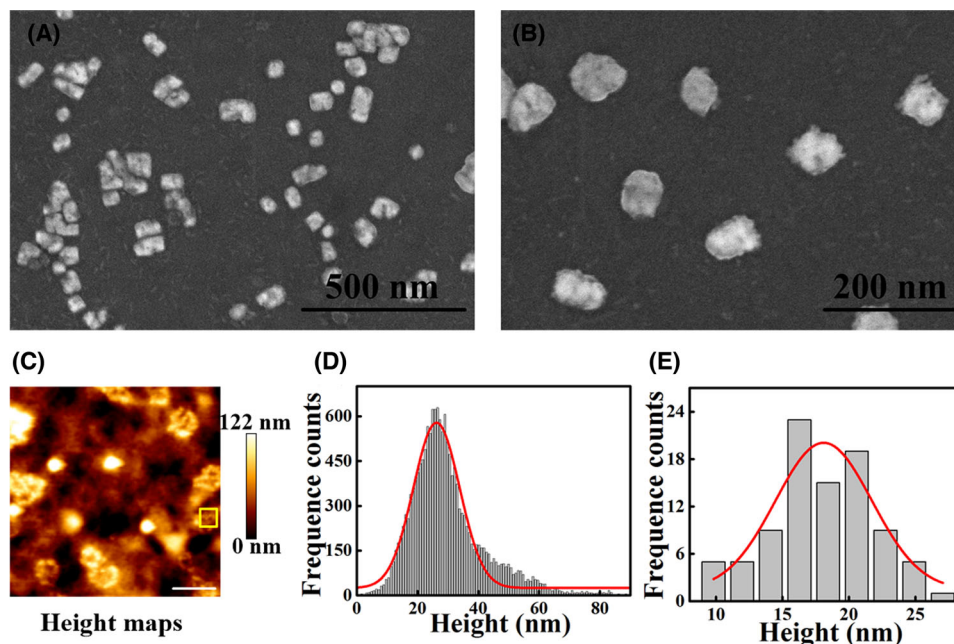
FIGURE 2 Morphological characterization of Ag nanoparticles: (A) typical FIB image with scale bar of 500 nm; (B) typical FIB image with scale bar of 200 nm; (C) AFM height map's image with a white scale bar of 1 μm, and the yellow square of 300 nm × 300 nm; (D) the statistical distribution corresponding to the whole AFM height map's image; (E) the statistical distribution corresponding to the selected statistical section of the yellow square of 300 nm × 300 nm in AFM height map's image. The red curves in (D) and (E) are the result after Gaussian distribution fitting.

of A549 cells and SMMC-7721 cells to investigate the effects of AgNPs on the morphological and mechanical properties of different cancerous cells.

3.3 | The effects of the concentrations of AgNPs on the morphological and mechanical properties of cell behaviours

Morphology is of great importance to investigate the physiological behaviour inside cells. The morphological properties of cells were carried out by inverted optical microscopy and AFM, respectively. Combining AFM with inverted optical microscopy enables the investigation of the morphology of live cancerous cells.

The optical graphics of the effects of the various concentrations of AgNPs of 0 μg/ml, 1.875 μg/ml, 3.75 μg/ml and 7.50 μg/ml on live cancerous cells of A549 cells and SMMC-7721 cells are demonstrated in Figure 3. The shapes of A549 cells and SMMC-7721 cells are both almost no changed with the increased concentrations of AgNPs, which exhibit as irregular spindle configurations and elliptical shape. In addition, the sizes of A549 and SMMC-7721 cells are within the general dimension ranges of previous studies, which are 50–90 and 35–55 μm in lengths, 25–40 μm in widths. However, the bright spots of both cancerous cells become visible and increased with the increase of the concentra-
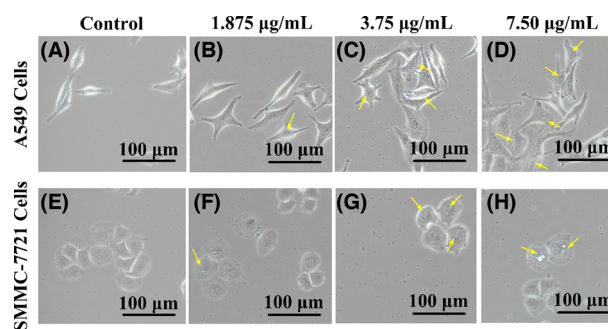

FIGURE 3 Optical images of A549 cells and SMMC-7721 cells with various concentrations of AgNPs: (A)–(D) optical images of A549 cells with AgNPs concentrations of 0, 1.875, 3.75 and 7.50 μg/ml, respectively; (E)–(H) optical images of SMMC-7721 cells with AgNPs concentrations of 0, 1.875, 3.75 and 7.50 μg/ml, respectively.

tion of AgNPs. The reason for this phenomenon possibly is that cell membranes have the opportunity to penetrate nanoparticles and cell internal components may interact with nanoparticles, which may appeared the possibility to induce destruction of the cell membrane and the apoptosis of cells. Therefore, the A549 cells and SMMC-7721 cells both appeared the visible bright spots with the stimulation of AgNPs from the inverted optical images.

Owing to the limitation of the inverted optical images of the changes of the morphology for A549 cells and
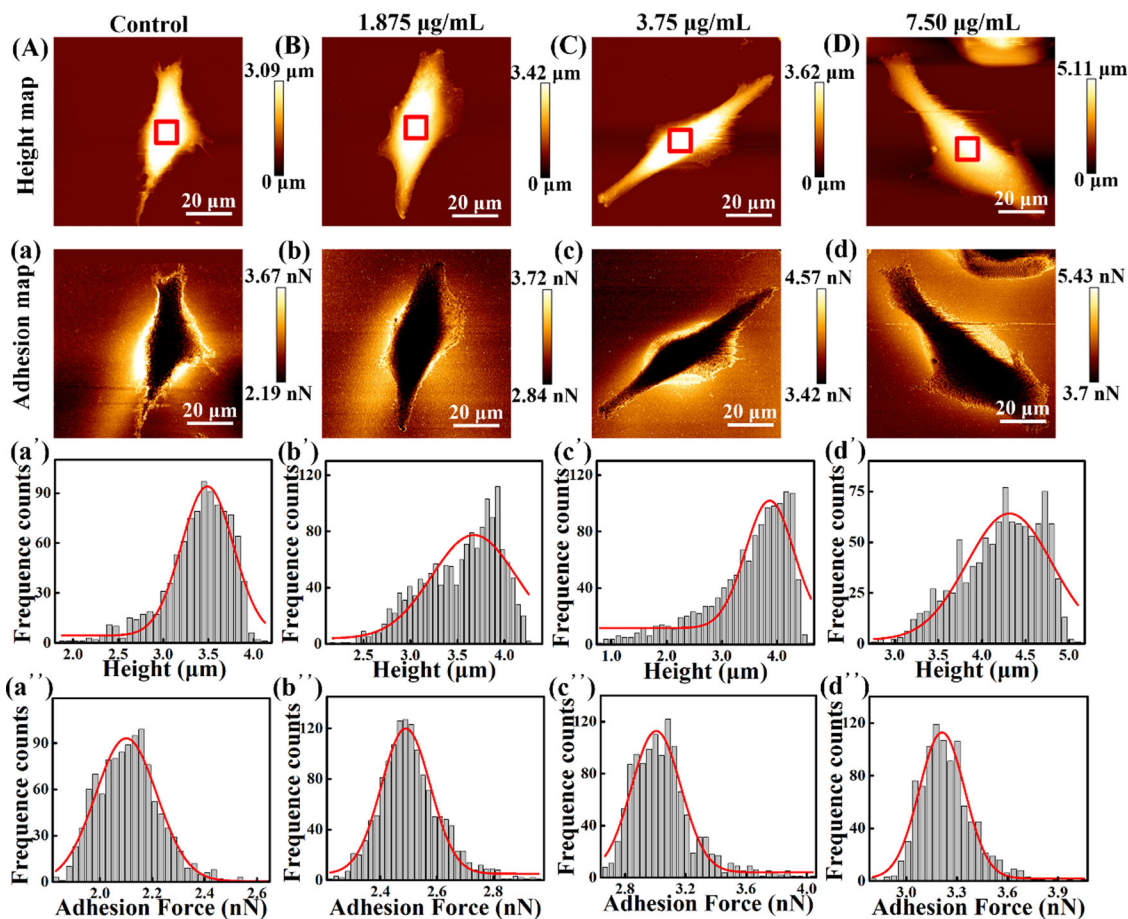
FIGURE 4 AFM images of a single live A549 cell with 256 × 256 pixels: (A)–(D) are the height maps of 0, 1.875, 3.75 and 7.50 μg/ml, respectively; (a)–(d) are the adhesion force maps of 0, 1.875, 3.75 and 7.50 μg/ml, respectively; (a')–(d') are the statistical distribution corresponding to the 10 μm × 10 μm selected statistical sections of height maps of 0, 1.875, 3.75 and 7.50 μg/ml, respectively; (a")–(d") are the statistical distribution corresponding to the 10 μm × 10 μm selected statistical sections of height maps of 0, 1.875, 3.75 and 7.50 μg/ml, respectively. The white scale bar is 20 μm. The red box in (A)–(D) is 10 μm × 10 μm. The red curves in (a')–(d') and (a")–(d") are the result after Gaussian distribution fitting.

SMMC-7721 cells, it is extremely difficult to compare the specific distinctions between the two cancerous cells with the stimulation of the various concentrations of AgNPs. Therefore, AFM analysis is essential to be applied in the following measurement with the more precise revolution in order to investigate the detailed effects of the increased concentrations of AgNPs on the morphological and mechanical properties of two types of cancerous cells.

The force–volume (FV) mode of JPK system (NanoWizard®3, Germany) is used to characterize the morphological properties of A549 cells and SMMC-7721 cells with the increased concentration of AgNPs, shown in Figures 4 and 5. The measurement parameters of indentation force, indentation speed were set to 1.0 nN and 2.0 μm/s in this scanning measurement in order to measure the height, roughness and adhesion force of A549 cells and SMMC-7721 cells. The resolution ratio

of AFM images is 256 × 256 pixels. The corresponding measurement time of a 256 × 256 pixels AFM image is 10–15 min. The scanning area covers the whole of a single A549 cell and SMMC-7721 cell. The samples of cultured cells on the concentration of AgNPs solutions of 0 μg/ml, 1.875 μg/ml, 3.75 μg/ml and 7.50 μg/ml for 24 h. In order to ensure the validity and accuracy, at least 10 cells were measured in the scanning measurement. It is important to note that in order to ensure cell viability, measurements need to be carried out as quickly as possible. Therefore, only one of the ten cells is at 256 × 256 pixels resolution while the others are at 64 or 128 pixels resolution, which is much faster scanning speed and less scanning time.

As revealed in Figures 4 and 5, the appearance of shapes of A549 cells and SMMC-7721 cells changes little. However, the height and adhesion force values are obviously increasing with the increasing concentration of AgNPs of
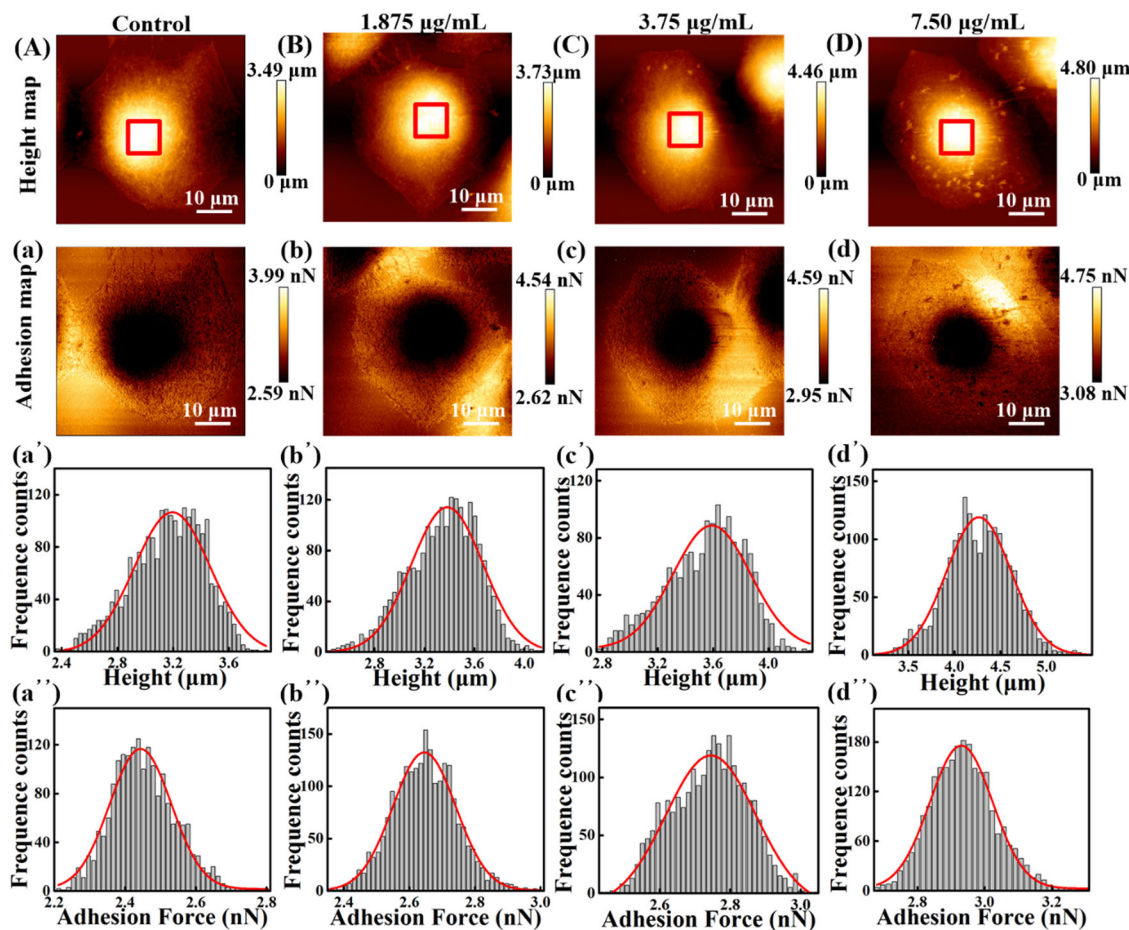
FIGURE 5 AFM images of a single live SMMC-7721 cell with 256 × 256 pixels: (A)–(D) are the height maps of 0, 1.875, 3.75 and 7.50 μg/ml, respectively; (a)–(d) are the adhesion force maps of 0, 1.875, 3.75 and 7.50 μg/ml, respectively; (a')–(d') are the statistical distribution corresponding to the 10 μm×10 μm selected statistical sections of height maps of 0, 1.875, 3.75 and 7.50 μg/ml, respectively; (a")–(d") are the statistical distribution corresponding to the 10 μm × 10 μm selected statistical sections of height maps of 0, 1.875, 3.75 and 7.50 μg/ml, respectively. The white scale bar is 10 μm. The red box in (A)–(D) is 10 μm × 10 μm. The red curves in (a')–(d') and (a")–(d") are the results after Gaussian distribution fitting.

0 μg/ml, 1.875 μg/ml, 3.75 μg/ml and 7.50 μg/ml. Additionally, the AFM results of height, roughness and adhesion force of A549 cells and SMMC-7721 cells are summarized in Figure 6.

The height values of the control group of A549 cells and SMMC-7721 cells of the AgNPs concentration of 0 μg/ml were 3.88 ± 0.26 μm and 4.15 ± 0.19 μm. For A549 cells, the height values of concentrations of 1.875 μg/ml, 3.75 μg/ml and 7.50 μg/ml varied to 4.38 ± 0.07 μm, 4.68 ± 0.11 μm and 5.38 ± 0.41 μm, respectively. With the increased concentration of AgNPs, it showed an obvious rising variation tendency. For SMMC-7721 cells, the height values of concentrations of 1.875 μg/ml, 3.75 μg/ml and 7.50 μg/ml increased to 4.18 ± 0.19 μm, 4.33 ± 0.47 μm and 5.03 ± 0.57 μm, respectively. However, the average height changed minor and then varied significantly with the concentration of 7.50 μg/ml. Therefore, the height of A549 cells and 7721 cells both increased with the increased concentra-

tions of AgNPs. Nevertheless, there are different variations in the height of two cancerous cells.

The roughness values of the control group of A549 cells and SMMC-7721 cells of the AgNPs concentration of 0 μg/ml were 1.15 ± 0.08 μm and 1.19 ± 0.06 μm. For A549 cells, the roughness values of concentrations of 1.875 μg/ml, 3.75 μg/ml and 7.50 μg/ml varied to 1.26 ± 0.07 μm, 1.35 ± 0.11 μm and 1.59 ± 0.15 μm, respectively. With the increased concentration of AgNPs, it shows an evident rising variation tendency. For SMMC-7721 cells, the roughness values of concentrations of 1.875 μg/ml, 3.75 μg/ml and 7.50 μg/ml increased to 1.27 ± 0.06 μm, 1.36 ± 0.11 μm and 1.41 ± 0.12 μm, respectively. However, the average roughness is not significantly different from the control group with the stimulation of concentration of 1.875 μg/ml while changing obviously with the increased concentration of 3.75 and 7.50 μg/ml. Therefore, the roughness of A549 cells and SMMC-7721 cells both increased with the increased
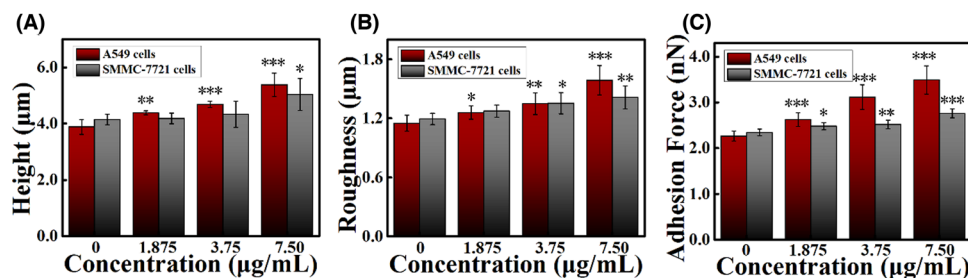
FIGURE 6 AFM results of A549 cells and SMMC-7721 cells with the concentrations of AgNPs of 0, 1.875, 3.75 and 7.50 μg/ml, respectively: (A) height; (B) roughness; (C) adhesion force. The differences between the experimental groups and the control group were considered statistically significant at *$p < 0.05$, **$p < 0.01$ and ***$p < 0.001$. The results are represented as the mean and standard deviation ($\pm$).

concentrations of AgNPs. Otherwise, different variations on the roughness of two cancerous cells are shown in the AFM images.

The adhesion force of the control group of A549 cells and SMMC-7721 cells of the AgNPs concentration of 0 μg/ml were 2.26 ± 0.11 nN and 2.34 ± 0.07 nN. For A549 cells, the adhesion force of concentrations of 1.875 μg/ml, 3.75 μg/ml and 7.50 μg/ml varied to 2.62 ± 0.15 nN, 3.12 ± 0.27 nN and 3.49 ± 0.31 nN, respectively. For SMMC-7721 cells, the adhesion force of concentrations of 1.875 μg/ml, 3.75 μg/ml and 7.50 μg/ml increased to 2.48 ± 0.08 nN, 2.52 ± 0.09 nN and 2.76 ± 0.10 nN, respectively. Therefore, the adhesion force of A549 cells and 7721 cells both increased with the increased concentrations of AgNPs. With the increased concentration of AgNPs, both cancerous cells showed an obvious rising variation tendency.

Therefore, the AgNPs has significant effects on the morphological and mechanical properties of A549 cells and SMMC-7721 cells. The values of height, roughness and adhesion force increased with the increased concentrations of AgNPs for A549 cells and 7721 cells. However, there are distinctive variations in the height, roughness of two cancerous cells while both cells have an obvious rising variation tendency on adhesion force. The reason for this phenomenon possibly due to the various cancerous cells with complicated intracellular structures may react changeable with the different concentrations of AgNPs, such as the cytoskeleton, filamentous actin, cell matrix etc. Moreover, nanoparticles are able to penetrate the cell membranes and interact with cell internal components. When AgNPs begin to contact the lipid membrane, it is possible to induce destruction of the cell membrane and extract phospholipid molecules from membrane, which may cause the apoptosis of cells. At present, the absorption of nanoparticles by cell membrane has been verified by theoretical and experimental methods.[15] In addition, the chemical receptor might cause the possible change of silicon probe-cell surface adhesion.[39] Therefore, the morphological properties of A549 cells and 7721 cells displayed

evident differences with the stimulation of AgNPs with AFM analysis, such as values of height, roughness and adhesion force.

3.4 | The effects of the concentrations of AgNPs on Young's moduli of cancerous cells

JPK force spectroscopy mode with sinusoidal waveforms accompanied the modulation frequency of 50 Hz is used in this nano-indentation measurement in order to characterize the effects of the concentrations of AgNPs on Young's moduli of cancerous cells of A549 cells and SMMC-7721 cells. The measurement area is the central nucleus of cells. The probe applied in this measurement is MLCT A with a triangular silicon nitride tip with the nominal spring constant of 0.07 N/m. Due to the sharpness of triangular probes, the Sneddon model is applied to the calculation of Young's moduli by fitting the approach force–distance curves. The measurement parameters of indentation force, indentation speed, dwelling time, retraction time and Z length were set to 1 nN, 2.0 μm/s, 0.0 s, 0.0 s and 5.0 μm, respectively. The samples were put in the PBS solutions and at least 5 force curves of over ten cells for each sample were obtained in this measurement to eliminate the potential environmental influence in order to ensure the validity and accuracy of experimental data. Each force–distance curve is carried out in several seconds (1–15 s when the indentation speed is 0.5–5 μm/s), thus the over 50 curves for each sample is usually completed in 10 min.

The fitting results of Young's moduli of A549 cells and SMMC-7721 cells are displayed in Figure 7. The approach force–distance curves of A549 cells and SMMC-7721 cells in 0 μg/ml, 1.875 μg/ml, 3.75 μg/ml and 7.50 μg/ml are depicted in Figure 7A and B, respectively. It can be seen that the slopes of approach force–distance curves of A549 cells and SMMC-7721 cells are changed to be increased with the increased concentration of AgNPs. To
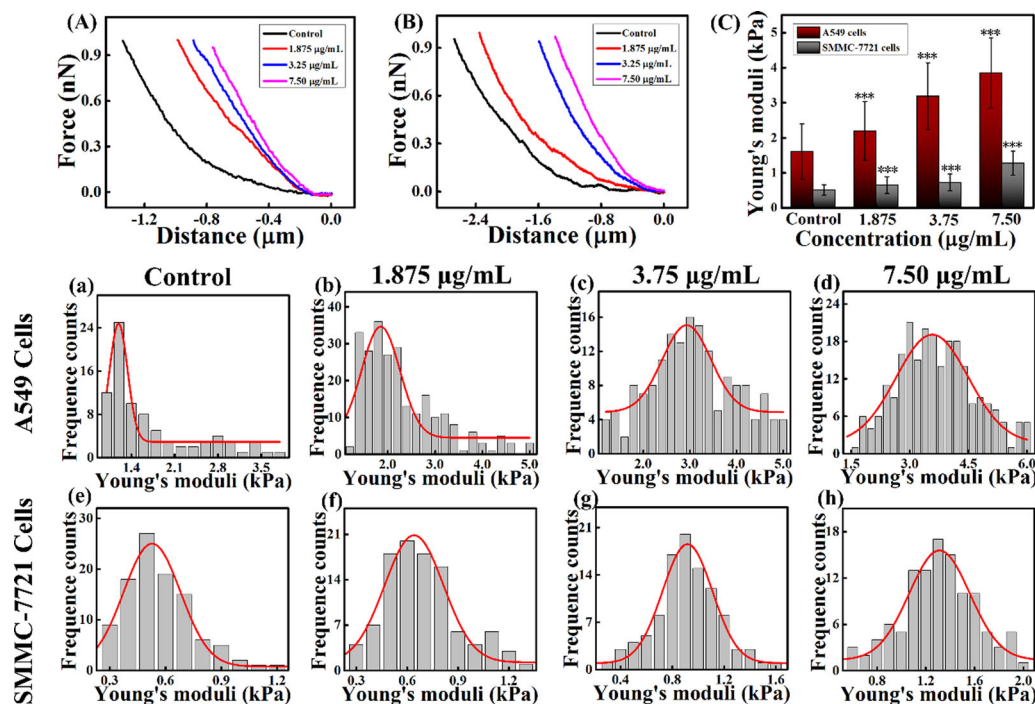
FIGURE 7 Fitting results of Young's moduli of A549 cells and SMMC-7721 cells based on Sneddon model: (A) Approach force–distance curves of A549 cells with the concentrations of AgNPs of 0, 1.875, 3.75 and 7.50 μg/ml, respectively. (B) Approach force–distance curves of SMMC-7721 cells with the concentrations of AgNPs of 0, 1.875, 3.75 and 7.50 μg/ml, respectively. (C) Fitting results of the average Young's moduli of A549 cells and SMMC-7721 cells; (a)–(d) are the statistical distribution of A549 cells' Young's moduli with the concentrations of AgNPs of 0, 1.875, 3.75 and 7.50 μg/ml, respectively; (e)–(f) are the statistical distribution of SMMC-7721 cells' Young's moduli with the concentrations of AgNPs of 0, 1.875, 3.75 and 7.50 μg/ml, respectively. The red curves in (a)–(h) are the results after Gaussian distribution fitting. The differences between the experimental groups and the control group were considered statistically significant at *$p < 0.05$, **$p < 0.01$ and ***$p < 0.001$. The results are represented as the mean and standard deviation ($\pm$).

be more specific, the slope of approach force–distance curves of A549 cells and SMMC-7721 cells increased with the increased concentration of AgNPs of 1.875 μg/ml, 3.75 μg/ml and 7.50 μg/ml.

Figure 7C shows the fitting results of the average Young's moduli of A549 cells and SMMC-7721 cells. The statistical distribution of A549 cells' and SMMC-7721 cells' Young's moduli of 0, 1.875 μg/ml, 3.75 μg/ml and 7.50 μg/ml are shown in Figure 7a–f. From the Figure 7C, the Young's moduli of control A549 cells and SMMC-7721 cells with the concentration of AgNPs of 0 μg/ml were 1.61 $\pm$ 0.79 kPa and 0.51 $\pm$ 0.15 kPa. For A549 cells, the Young's moduli with the concentration of AgNPs of 1.875 μg/ml, 3.75 μg/ml and 7.50 μg/ml varied to 2.20 $\pm$ 0.83 kPa, 3.19 $\pm$ 1.15 kPa, 3.85 $\pm$ 1.00 kPa, respectively. For SMMC-7721 cells, the Young's moduli with the concentration of AgNPs of 1.875 μg/ml, 3.75 μg/ml and 7.50 μg/ml increased to 0.65 $\pm$ 0.24 kPa, 0.73 $\pm$ 0.24 kPa and 1.28 $\pm$ 0.34 kPa, respectively. With the increased concentration of AgNPs, both cancerous cells of A549 cells and SMMC-7721 cells showed a visible rising variation tendency.

To sum up, the Young's moduli of A549 cells and SMMC-7721 cells both increased compared to that of the control

group. Moreover, the Young's moduli values of both two cancerous cells increased with the increased concentration of AgNPs of 1.875 μg/ml, 3.75 μg/ml and 7.50 μg/ml. Therefore, the concentration of AgNPs has significant effects on the Young's moduli of A549 cells and SMMC-7721 cells. With the increased concentration of AgNPs, both cancerous cells showed an obvious rising variation tendency. The possible reason for this phenomenon is AgNPs may inhibit some cellular activities with potential damages of complicated intracellular structures. With the increasing concentrations of AgNPs, it raises the possibility to accelerate the interior damages and apoptosis of cancerous cells. It has been verified by theoretical and experimental methods that cell membranes have the ability to penetrate nanoparticles and cell internal components may interact with nanoparticles, which may appeared the possibility to induce destruction of the cell membrane, extract phospholipid molecules from the membrane and cause the apoptosis of cells.[15] Therefore, the mechanical properties of A549 cells and 7721 cells appeared obvious differences with the stimulation of AgNPs utilizing the force spectroscopy mode, especially for the values of Young's moduli.

4 | CONCLUSIONS

We investigated the mechanical effects of AgNPs on cancerous cells of A549 cells and SMMC-7721 cells based on atomic force microscopy. The effects of AgNPs on the morphological properties and mechanical properties of cancerous cells were characterized by utilizing the force–volume (FV) mode and force spectroscopy mode based on AFM methodologies. We mainly focus on the comparison of the effects of AgNPs on the two types of cancerous cells with emphasis on the fitting results of calculating the Young's moduli based on Sneddon model. The results showed that the appearance of shapes of A549 cells and SMMC-7721 cells changes little to react with the various concentrations of AgNPs. However, the height, roughness, adhesion force and Young's moduli values increased with the increased concentration of AgNPs of 0 μg/ml, 1.875 μg/ml, 3.75 μg/ml and 7.50 μg/ml. This research has provided insights into the classification and characterization of the effects of the various concentrations of AgNPs on the cancerous cells in vitro utilizing AFM methodologies for disease therapy.

CONFLICT OF INTEREST

There are no conflicts of interest to declare.

ORCID

Yanling Tian https://orcid.org/0000-0001-8859-2124
Zuobin Wang https://orcid.org/0000-0002-7168-0918

REFERENCES

1. Baudrimont, M., Andrei, J., Mornet, S., Gonzalez, P., Mesmer-Dudons, N., Gourves, P. Y., & Feurtet-Mazel, A. (2018). Trophic transfer and effects of gold nanoparticles (AuNPs) in *Gammarus fossarum* from contaminated periphytic biofilm. *Environmental Science and Pollution Research*, *25*, 11181–11191.
2. Iriarte-Mesa, C., López, Y. C., Matos-Peralta, Y., de la Vega-Hernández, K., & Antuch, M. (2020). Gold, silver and iron oxide nanoparticles: Synthesis and bionanoconjugation strategies aimed at electrochemical applications. *Topics in Current Chemistry*, *378*(1), 12.
3. Mylona, Z., Panteris, E., Kevrekidis, T., & Malea, P. (2020). Silver nanoparticle toxicity effect on the *Seagrass halophilastipulacea*. *Ecotoxicology and Environmental Safety*, *189*, 109925.
4. Gorrochategui, E., Li, J., Fullwood, N. J., Ying, G. G., Tian, M., Cui, L., & Martin, F. L. (2017). Diet-sourced carbon-based nanoparticles induce lipid alterations in tissues of zebrafish (*Danio rerio*) with genomic hypermethylation changes in brain. *Mutagenesis*, *32*(1), 91–103.
5. Hu, Q., Pan, Y., Gong, X., Rao, S. Q., Xiao, L., Liu, L., & Yang, Z. Q. (2020). A sensitivity enhanced fluorescence method for the detection of ferrocyanide ions in foodstuffs using carbon nanoparticles as sensing agents. *Food Chemistry*, *308*, 125590.
6. Meeker, D. G., Wang, T., Harrington, W. N., Zharov, V. P., Johnson, S. A., Jenkins, S. V., & Smeltzer, M. S. (2018). Versatility of targeted antibiotic-loaded gold nanoconstructs for the treatment of biofilm-associated bacterial infections. *International Journal of Hyperthermia*, *34*(2), 209–219.
7. Sengan, M., Subramaniyan, S. B., Arul, P. S., Ravi, K. K., & Veerappan, A. (2019). Effective elimination of biofilm formed with waterborne pathogens using copper nanoparticles. *Microbial Pathogenesis*, *127*, 341–346.
8. de Mélo Silva, I. S., do Amorim Costa Gaspar, L. M., Rocha, A. M. O., da Costa, L. P., Tada, D. B., Franceschi, E., & Padilha, F. F. (2020). Encapsulation of red propolis in polymer nanoparticles for the destruction of pathogenic biofilms. *Aaps Pharmscitech [Electronic Resource]*, *21*, 49.
9. Prasad, R., Siddhardha, B., & Dyavaiah, M. (2020). *Nanostructures for antimicrobial and antibiofilm applications.* Springer International Publishing, ISBN 978-3-030-40336-2.
10. Prasad, R. (2014). Synthesis of silver nanoparticles in photosynthetic plants. *Journal of Nanoparticles*, *2014*, 963961.
11. Prasad, R., Pandey, R., & Barman, I. (2016). Engineering tailored nanoparticles with microbes: Quo vadis. *WIREs Nanomedicine and Nanobiotechnology*, *8*, 316–330.
12. Ealia, S. A. M., & Saravanakumar, M. P. (2017). A review on the classification, characterization, synthesis of nanoparticles and their application. *IOP Conference Series: Materials Science and Engineering*, *263*(3), 032019.
13. Kumari, S., Yadav, B. S., & Yadav, R. B. (2020). Synthesis and modification approaches for starch nanoparticles for their emerging food industrial applications: A review. *Food Research International*, *128*, 108765.
14. Azeredo, H. M. C., Otoni, C. G., Corrêa, D. S., Assis, O. B. G., Moura, M. R. D., & Mattoso, L. H. C. (2019). Nanostructured antimicrobials in food packaging-recent advances. *Biotechnology Journal*, *14*, 1900068.
15. Wu, R. R., Ou, X. W., Tian, R. R., Zhang, J., Jin, H. S., Dong, M. D., & Liu, L. (2018). Membrane destruction and phospholipid extraction by using two-dimensional mos2 nanosheets. *Nanoscale*, *10*, 20162–20170.
16. Singh, R. P., & Ramarao, P. (2012). Cellular uptake, intracellular trafficking, and cytotoxicity of silver nanoparticles. *Toxicology Letters*, *213*, 249–259.
17. Gholamrezazadeh, M., Shakibaie, M. R., Monirzadeh, F., Masoumi, S., & Hashemizadeh, Z. (2018). Effect of nano-silver, nano-copper, deconex and benzalkonium chloride on biofilm

formation and expression of transcription regulatory quorum sensing gene (rh1R) in drug-resistance *Pseudomonas aeruginosa* burn isolates. *Burns*, *44*(3), 700–708.

18. Meza-Villezcas, A., Gallego-Hernández, A. L., Yildiz, F. H., Jaime-Acuña, O. E., Raymond-Herrera, O., & Huerta-Saquero, A. (2019). Effect of antimicrobial nanocomposites on vibriocholerae lifestyles: Pellicle biofilm, planktonic and surface-attached biofilm. *PLoS ONE*, *14*(6), e0217869.

19. Meier, M. J., Dodge, A. E., Samarajeewa, A. D., & Beaudette, L. A. (2020). Soil exposed to silver nanoparticles reveals significant changes in community structure and altered microbial transcriptional profiles. *Environmental Pollution*, *258*, 113816.

20. Zou, X., Li, P., Wang, X., Zheng, S., Dai, F., & Zhang, H. (2020). Silver nanoparticle and Ag$^+$ induced shifts of microbial communities in natural brackish waters: Are they more pronounced under oxic conditions than anoxic conditions? *Environmental Pollution*, *258*, 113686.

21. Mapara, N., Sharma, M., Shriram, V., Bharadwaj, R., Mohite, K. C., & Kumar, V. (2015). Antimicrobial potentials of helicteresisora silver nanoparticles against extensively drugresistant (XDR) clinical isolates of *Pseudomonas aeruginosa*. *Applied Microbiology and Biotechnology*, *99*, 10655–10667.

22. Singh, R., Nawale, L. U., & Arkile, M. (2015). Chemical and biological metal nanoparticles as antimycobacterial agents: A comparative study. *International Journal of Antimicrobial Agents*, *46*, 183–188.

23. El-Zahry, M. R., Mahmoud, A., Refaat, I. H., Mohamed, H. A., Bohlmann, H., & Lendl, B. (2015). Antibacterial effect of various shapes of silver nanoparticles monitored by SERS. *Talanta*, *138*, 183–189.

24. Actis, L., Srinivasan, A., Lopez-Ribot, J. L., Ramasubramanian, A. K., & Ong, J. L. (2015). Effect of silver nanoparticle geometry on methicillin susceptible and resistant *Staphylococcus aureus*, and osteoblast viability. *Journal of Materials Science: Materials in Medicine*, *26*, 215.

25. Sinha, R., Karan, R., Sinha, A., & Khare, S. K. (2011). Interaction and nanotoxic effect of ZnO and Ag nanoparticles on mesophilic and halophilic bacterial cells. *Bioresource Technology*, *102*(2), 1516–1520.

26. Dufrene, Y. F. (2004). Using nanotechniques to explore microbial surfaces. *Nature Reviews Microbiology*, *2*(6), 451–460.

27. Muller, D. J., & Dufrene, Y. F. (2008). Atomic force microscopy as a multifunctional molecular toolbox in nanobiotechnology. *Nature Nanotechnology*, *3*(5), 261–269.

28. Yuan, S., Liu, L., Wang, Z., & Xi, N. (2020). *AFM-based observation and robotic nano-manipulation*. Beijing: Springer Science Press.

29. Yang, X. G., & Yang, X. (2012). *Atomic force microscopy*. Beijing: Chemical Industry Press.

30. Reimer, L. (2000). *Scanning electron microscopy: Physics of image formation and microanalysis* (Vol. 11, p. 1826, 2nd edn.). IOP Publishing Ltd.

31. DB, W., & Carter, C. B. (1996). *Transmission electron microscopy: A textbook for materials science*. Germany: Plenum Press, Springer.

32. Dupres, V., Alsteens, D., Wilk, S., Hansen, B., Heinisch, J. J., & Dufrêne, Y. F. (2009). The yeast wsc1 cell surface sensor behaves like a nanospring in vivo. *Nature Chemical Biology*, *5*(11), 857–862.

33. Dague, E., Alsteens, D., Latgé, J. P., & Dufrêne, Y. F. (2008). High-resolution cell surface dynamics of germinating *Aspergillus fumigatus* conidia. *Biophysical Journal*, *94*(2), 656–660.

34. Scheuring, S., & Sturgis, J. N. (2005). Chromatic adaptation of photosynthetic membranes. *Science*, *309*(5733), 484–487.

35. Engel, A., & Muller, D. J. (2000). Observing single biomolecules at work with the atomic force microscope. *Nature Structural & Molecular Biology*, *7*(9), 715–718.

36. Dufrêne, Y. F., Ando, T., Garcia, R., Alsteens, D., Martinez-Martin, D., Engel, A., & Müller, D. J. (2017). Imaging modes of atomic force microscopy for application in molecular and cell biology. *Nature Nanotechnology*, *12*(4), 295–307.

37. Kirmizis, D., & Logothetidis, S. (2010). Atomic force microscopy probing in the measurement of cell mechanics. *International Journal of Nanomedicine*, *5*(1), 137–145.

38. Aroush, D. R. B., Asnacios, A., Chen, W. C., Dokukin, M. E., Doss, B. L., Durand, P., & Wirtz, D. (2018). Comparative study of cell mechanics methods. *Nature Methods*, *15*(7), 491–498.

39. Lazar, P., Zhang, S., Šafářová, K., Li, Q., Froning, J. P., Granatier, J., & Otyepka, M. (2013). Quantification of the interaction forces between metals and graphene by quantum chemical calculations and dynamic force measurements under ambient conditions. *ACS Nano*, *7*(2), 1646–1651.